Origin of Electrical Instabilities in Self-Aligned Amorphous In–Ga–Zn–O Thin-Film Transistors

Nuri On, Youngho Kang, Aeran Song, Byung Du Ahn, Hye Dong Kim, Jun Hyung Lim, Kwun-Bum Chung[ID], Seungwu Han, and Jae Kyeong Jeong[ID]

Abstract— **This paper examined the performance and bias stability of amorphous In–Ga–Zn–O (*a*-IGZO) thin-film transistors (TFTs) with a self-aligned coplanar structure. The activation energy barrier responsible for the positive bias thermal stress (PBTS)-induced instability of the *a*-IGZO TFTs with low oxygen loadings can be attributed to the migration of cation interstitial defects. However, the IGZO TFTs with high oxygen loadings could not be explained by the existing defect model. The first-principle calculation indicates that the cation vacancy, such as V_{In}, with the hydrogen incorporation plays an important role in determining the PBTS-dependent degradation of the threshold voltage.**

Index Terms— **Amorphous In–Ga–Zn–O (*a*-IGZO), cation interstitial, instability, oxygen vacancy, thin-film transistor (TFT).**

I. INTRODUCTION

AMORPHOUS indium gallium zinc oxide (*a*-IGZO) has extensively been studied for use as active channel material in thin-film transistors (TFTs) for active-matrix electronics of liquid crystals and organic light-emitting diodes screens [1]–[5] Effective intercalation of the nondirectional *ns* orbital of metal cations and the amorphous metal-oxide (M-O) network with a strong ionicity enable reasonably high carrier mobility, moderate stability, and large-area uniformity of these compounds. Despite these attractive features, the electrical instability of IGZO TFTs is still a critical hurdle against widespread commercialization of the devices [6]. Various degradation mechanisms have been intensively investigated as an intrinsic origin, including the oxygen vacancy (V_O) [7]–[15], zinc interstitial (Zn_i) [16], oxygen interstitial (O_i) [5], [17], [18], and hydrogen bistability [19] models. These studies have mainly focused on

the bottom gate architecture, which is preferred due to the simple fabrication process. However, the staggered structure, such as the bottom gate architecture, has an electrode overlap to facilitate the charge carrier injection from the source into the channel layer. This parasitic capacitance [20] causes a delay in the visual signal and aggravates the undesirable visual artifacts such as flickering and image sticking. Therefore, self-aligned IGZO TFTs should be developed to satisfy the stringent requirement of the next-generation high-pixel densities and large screens. Notwithstanding the technical importance, the electrical instability of the self-aligned IGZO TFTs has been rarely examined [5]. In this paper, we report the degradation mechanism of the threshold voltage (V_{TH}) under the gate bias thermal stress conditions for self-aligned TFTs with sputtered IGZO channels prepared at different oxygen loadings conditions. The positive gate bias thermal stress (PBTS)-dependent instability of the IGZO devices deteriorated with increasing oxygen loadings [(flow ratio) of $[O_2]/([Ar] + [O_2])$]. The origin for the oxygen loadings-dependent PBTS instability was proposed on the basis of the activation energy barrier analysis. The IGZO device with lower oxygen loadings can be attributed to the migration of cation interstitial defects whereas the formation of the cation vacancy defects was identified as a plausible degradation mechanism for the IGZO device with higher oxygen loadings.

II. EXPERIMENTAL PROCEDURE

The evaluated IGZO TFTs had the self-aligned coplanar structure. A SiO_2/SiN_x buffer layer was deposited on the glass substrate using plasma-enhanced chemical vapor deposition (PECVD). A 20-nm-thick *a*-IGZO channel layer was sputtered using a polycrystalline $In_2Ga_2ZnO_7$ target, where the oxygen loadings during the thin-film preparation was split into 63%, 75%, and 80% of the $[O_2]/([Ar] + [O_2])$. The cation ratio of the IGZO films was In: Ga: Zn = 2.2: 2.2: 1.0. A 120-nm-thick SiO_2 film as a gate dielectric was deposited by PECVD on the a-IGZO/SiO_2/SiN_x/Glass substrate, which was followed by the coating of Cu film as a gate electrode using dc sputtering. The definition of the gate electrode was performed by the traditional lithography and dry etching. A SiO_2 film was deposited as an interlayer by PECVD and the contact hole was opened for a source/drain (S/D) metallization. Finally, the Mo/Al stack was deposited and patterned as the S/D electrodes, which was followed by thermal annealing
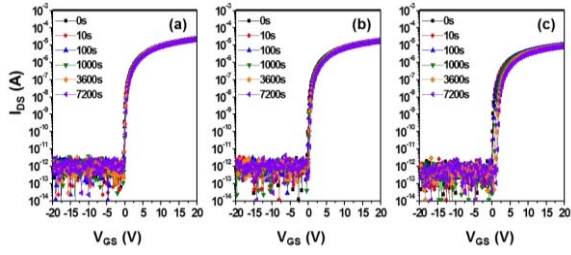
Fig. 1. Evolution of the transfer curves for a-IGZO TFTs with oxygen loadings of (a) 63%, (b) 75%, and (c) 80% as a function of PBTS time.
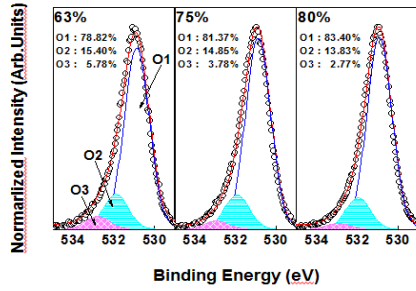

Fig. 2. Chemical characterization of IGZO films with different oxygen loadings. Deconvoluted XPS spectra of the O 1s core level of the IGZO films.

Fig. 3. Electronic structure of the IGZO films. Variations in the (a) absorption coefficient (α) measured by spectroscopic ellipsometry and (b) VB spectra by XPS. (c) Schematic energy band diagrams reflecting the relative energy position of the Fermi level (E_F) with respect to the CB minimum (E_{CB}) and VB maximum (E_{VB}) for the IGZO film with different oxygen loadings of 63%, 75%, and 80%. (d) Variation in the DOS below E_{CB} for the IGZO TFTs. DOS distributions were extracted based on the MN rule.

at 200 °C. Electrical characterization was carried out using a Keithley 2636 parameter analyzer. The field-effect mobility (μ_{FE}) was determined from the maximum incremental slope of an $I_{DS}^{1/2}$ versus V_{GS} plot in the saturation region according to the following equation: $I_{DS} = (WC_i/2L)\mu_{FE}(V_{GS}-V_{TH})^2$, where L is the channel length, W is the width, and C_i is the gate capacitance per unit area. The V_{TH} was determined from the gate voltage (V_{GS}) needed to produce a drain current of $L/W \times 10$ nA at $V_{DS} = 5.1$ V. The subthreshold gate swing ($SS = dV_{GS}/d \log I_{DS}$) was extracted from the linear portion of a plot of the log I_{DS} versus V_{GS}.

III. RESULTS AND DISCUSSION

Fig. 1 shows the evolution of $I_{DS}-V_{GS}$ characteristics for a-IGZO TFTs with different oxygen loadings of 63%, 75%, and 80% as a function of PBTS time. The gate bias stresses of 20 V were applied at room temperature in air. The gate bias was interrupted at fixed times to record the IV curves of the devices, which was measured at a V_{DS} of 5.1 V. The pristine device characteristics correspond to the $I_{DS}-V_{GS}$ measured at 0 s (before stress). The device with 63% oxygen loadings exhibited a reasonable field-effect mobility (μ_{FE}) of 9.8 cm²/Vs, subthreshold gate swing (SS) of 0.27 V/decade, threshold voltage (V_{TH}) of 0.0 V, and $I_{ON/OFF}$ ratio of 10^8 [Fig. 1(a)]. The carrier mobility was slightly diminished with increasing oxygen loadings: the device with 80% oxygen loadings had a μ_{FE} value of 6.8 cm²/Vs. Simultaneously, the SS and V_{TH} values for this device increased to 0.31 V/decade and 0.4 V, respectively, whereas a comparable $I_{ON/OFF}$ ratio was maintained [Fig. 1(c)].

In order to obtain the insight on the oxygen loadings-dependent electrical properties, the chemical states for the IGZO films were examined by the X-ray photoelectron spectroscopy (XPS). Fig. 2 shows the core level spectra of O 1s
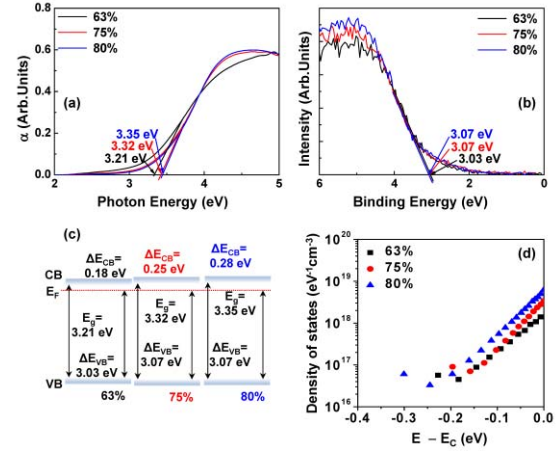
of the IGZO films with different oxygen loadings. XPS was obtained after sputtering by Ar ions at 500 eV to minimize the surface contamination of the adsorbed OH, C, H₂O, and other molecules. The oxygen signals were carefully deconvoluted with three different Gaussian bases (indexed as O1, O2, and O3) from a low binding energy. The O 1s peaks centered at 531 (O1) and 532 eV (O2) were assigned to fully coordinated oxygen and insufficiently coordinated oxygen (referred to as an oxygen vacancy [14], [15], V_O) with cations, respectively. The higher binding energy peak (O3) at 533 eV was attributed to oxygen impurities. The relative area of the oxygen deficient peak (O2) slightly decreased with increasing oxygen loadings. The IGZO films with higher oxygen loadings have smaller oxygen deficient states due to V_O, which is responsible for the reduction in free electron density and results in slight deterioration of the carrier transport.

Fig. 3(a) and (b) shows the unoccupied states near the conduction band (CB) and the occupied states near the valence band (VB) of IGZO films with different oxygen loadings, respectively. The extracted band gap increased from 3.21 to 3.35 eV and the VB offset (E_{VB}) between the Fermi level (E_F) and VB maximum (E_{VB}) slightly increased from 3.03 to 3.07 eV with increasing oxygen loadings. Considering the band gap (by spectroscopic ellipsometry) and VB offset (by XPS), a schematic energy diagram was obtained, as shown in Fig. 3(c). The CB offset (E_{CB}) between the CB minimum (E_{CB}) and E_F changed from 0.18 eV (oxygen loading: 63%) to 0.28 eV (oxygen loadings: 80%), which makes the transition from the localized trap-mediated transport to the percolation conduction difficult. In addition, the increase in CB offset (E_{CB}) is related to the decrease in the free electron density (n) by the following equation: $n = N_C e^{-(E_{CB}-E_F)/k_B T} n = N_C e^{-(E_{CB}-E_F)/kT}$, where N_C is the effective density of states near the E_{CB} and k_B is the Boltzmann's constant, and T is the absolute temperature. This result can be plausible rationale for the performance

This article has been accepted for inclusion in a future issue of this journal. Content is final as presented, with the exception of pagination.

ON *et al.*: ORIGIN OF ELECTRICAL INSTABILITIES

3

deterioration (such as μ_{FE} and V_{TH}) of a device with high oxygen loadings.

Temperature-dependent field-effect data were used to calculate the total density-of-state (DOS) [21] distributions in the forbidden band gap of the IGZO TFTs. The V_{TH} value for all the devices shifted negatively with increasing measurement temperature. This negative V_{TH} shift with increasing temperature can be interpreted by the thermal activation process of the subthreshold drain current (I_{DS}) from the quasi-Fermi level to the CB edge. Generally, the subthreshold current in the IGZO TFTs can be well described by the thermally activated Arrhenius model, where it was assumed that thermally activated electrons from a deep level trap site into the CB move quickly toward the drain electrode due to a lateral electrical field. Fig. 3(d) shows the DOS distributions based on the Meyer–Neldel (MN) [22], [23] rule, where the same procedure was used to calculate the DOS distribution [24]. The overall DOS distribution for the IGZO TFTs increased with increasing oxygen loadings over the entire tailing energy range extracted: the DOS values at the CB edge for the devices with oxygen loadings of 63%, 75%, and 80% were 1.4×10^{18}, 3.4×10^{18}, and 5.8×10^{18} ev^{-1} cm^3, respectively. It is noted that the largest DOS distribution for the device with 80% oxygen loadings is consistent with its largest SS factor in Fig. 1. This result suggests that the high oxygen loadings into the amorphous IGZO film not only annihilated the oxygen deficient defect, but also created some tailing states near the CB edge. Considering that the tail states in the bandgap are generally originated from the structural disordering in amorphous semiconducting material and the CB in IGZO is associated with intercalation of In *5s* orbital, the CB tail states can be related to the cation disordering. The higher oxygen loading in *a*-IGZO film may affect adversely the degree of cation disordering, which results in the increasing CB tail state below E_{CB}.

The effects of the application of PBTS on the transfer characteristics were investigated. The IGZO TFT with 63% oxygen loadings showed stable behavior against the external PBTS ($\Delta V_{TH} = 0.33$ V), as shown in Fig. 1(a). Notably, the PBTS-induced instability of the IGZO TFTs was deteriorated with increasing oxygen loadings. For example, the device with 80% oxygen loadings suffered from an enhanced V_{TH} shift ($\Delta V_{TH} = 1.57$ V) after identical PBTS duration (7200 s) [Fig. 1(c)]. The effect of the application of negative gate bias thermal stress (NBTS) on the device performance of IGZO TFTs was also investigated. The gate bias stresses of -20 V were applied: the other conditions were identical to the PBTS experiment. The pristine IGZO TFTs irrespective of the oxygen loadings turned out is very stable against the NBTS duration (Table I). The variations in the transfer characteristics for the IGZO TFTs with different oxygen loadings as a function of NBTS temperature and time were for example, the ΔV_{TH} values for the device with oxygen loadings of 63% were -0.06, -0.03 and -0.16 V for the measurement temperature of 60 °C, 80 °C, and 100 °C, respectively, after the application of NBTS for 7200 s (not shown). The other devices with different oxygen loadings of 75% and 80% exhibited negligible variations in term of V_{TH} shift after the identical NBTS
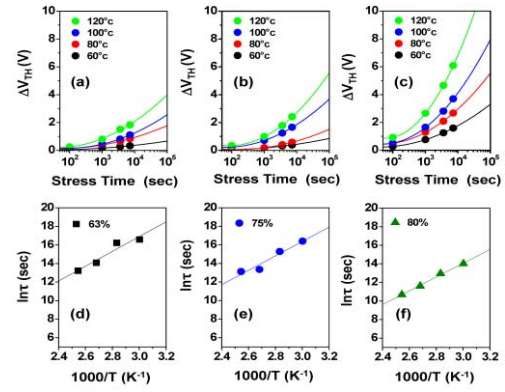

Fig. 4. Stretched exponential analysis for PBTS-induced instabilities of the IGZO TFTs. Temperature-dependent V_{TH} variations for the devices with oxygen loadings of (a) 63%, (b) 75%, and (c) 80% under the PBTS conditions. Relationship between $1/T$ versus $\ln\tau$ for the devices with oxygen loadings of (d) 63%, (e) 75%, and (f) 80%.

duration. These results indicated that our set of IGZO TFTs is highly stable under NBTS condition, which is consistent with those for the self-aligned IGZO TFTs in the previous reports [5].

Temperature-dependent stretched exponential analysis was performed to identify the plausible degradation mechanism for the IGZO TFTs with different oxygen loadings. The activation energy barriers ($E_\tau s$) extracted from this analysis help to elucidate the nature of the defect structure, where the density functional theory (DFT) calculation can be compared to the experimental barrier. Fig. 4 shows the variations in the V_{TH} values as a function of the PBTS time where the measuring temperatures were 60 °C, 80 °C, 100 °C, and 120 °C. These values were fit with a stretched exponential of the form: [25], [26]

$$|\Delta V_{th}(t)| = V_0 \left\{ 1 - \exp\left[-\left(\frac{t}{\tau}\right)^\beta \right] \right\} \quad (1)$$

where τ is the relaxation time, β is the dispersion parameter of the barrier energy height, and V_0 is $V_{GS} - V_{TH0}$ (V_{TH0} is the initial V_{TH} value). The relaxation time is given according to the following equation:

$$\tau = \nu^{-1} \exp\left(\frac{E_\tau}{k_B T}\right) \quad (2)$$

where ν is the frequency prefactor for emission over the barrier. The τ values from the fit of the stretched exponential to the data at 60 °C were calculated as 9.96×10^7, 1.33×10^7, and 1.09×10^7 for the IGZO TFTs with oxygen loadings of 63%, 75%, and 83%, respectively, whereas the β values 0.44–0.47 were independent of the oxygen loadings (Table II). The variations of $\ln\tau$ as a function of $1/T$ are shown in Fig. 4 for the IGZO TFTs with different oxygen loadings. The good fitting between $1/T$ versus $\ln\tau$ indicates that the PBTS-induced V_{TH} shift is a thermally activated process. Therefore, the extracted activation energy ($E_{\tau,PBTS}$) for each IGZO device can be interpreted as the energy required for the configurationally changes of the defect states, which is responsible for the dominant V_{TH} instability. The $E_{\tau,PBTS}$

This article has been accepted for inclusion in a future issue of this journal. Content is final as presented, with the exception of pagination.

4   IEEE TRANSACTIONS ON ELECTRON DEVICES
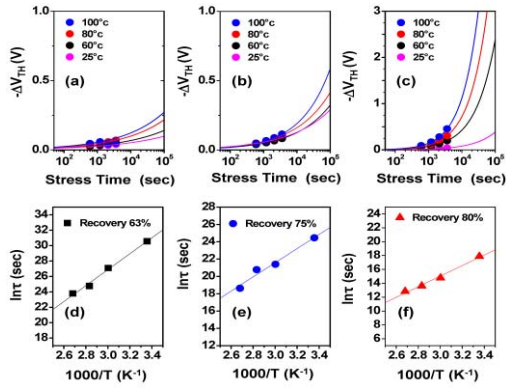

Fig. 5. Stretched exponential analysis for NBTS recovery for the IGZO TFTs. Temperature-dependent V_{TH} variations for the devices with oxygen loadings of (a) 63%, (b) 75%, and (c) 80% under the NBTS conditions. Relationship between $1/T$ versus $\ln\tau$ for the devices with oxygen loadings of (d) 63%, (e) 75%, and (f) 80%.

TABLE I

V_{TH} SHIFT DATA AFTER NBTS FOR PRISTINE DEVICES AND NBTS RECOVERY (APPLICATION OF NBTS AFTER PBTS) FOR a-IGZO TFTs

BTS condition	Temperature (°C)	ΔV_{TH} (V)		
		63%	75%	80%
NBTS (3600s)	60	-0.01	-0.07	-0.04
	80	-0.02	-0.08	-0.09
	100	-0.06	-0.07	-0.08
NBTS-recovery (3600s)	25	-0.04	-0.09	-0.08
	60	-0.05	-0.09	-0.13
	80	-0.07	-0.11	-0.21
	100	-0.09	-0.12	-0.29

value of the IGZO TFTs with oxygen loadings of 63%, 75%, and 80% was evaluated as approximately 0.87, 0.67, and 0.63 eV, respectively.

Next, we examined the NBTS recovery behavior of the IGZO TFTs with different oxygen loadings. First, the devices were subjected to the application of PBTS at 25 °C, 60 °C, 80 °C, and 100 °C for 1 h. To accelerate the displacement of transfer curves for all the devices to the negative gate voltage direction, the stress of negative 30 V was applied to the gate electrode ($V_{GS,ST} = -30$ V) for 3600 s. Fig. 5 shows the NBTS recovery time-dependent V_{TH} and the relaxation time variations. The $E_{\tau,\text{NBTS recovery}}$ values for the IGZO TFTs with different oxygen loadings of 63%, 75%, and 80% were 0.89, 0.70, and 0.65 eV, respectively. Because the NBTS duration for the pristine IGZO TFTs did not affect the I_{DS}–V_{GS} characteristics aforementioned, the V_{TH} by the application of NBTS recovery after prolonged PBTS duration is believed to come from the reverse process for the PBTS-induced degradation mechanisms.

The effectiveness of the energy barriers extracted from the stretched exponential analysis was confirmed using the Laplace transform technique [27]. The Lorentz curve with the most probable barrier energy at 0.81 eV was obtained for the device with the oxygen loadings of 63% (data not shown).

TABLE II

SUMMARY FOR THE τ, β AND E_τ VALUES UNDER PBTS AND NBTS RECOVERY FOR a-IGZO TFTs. THE τ AND β VALUES WERE EXTRACTED FROM EXPERIMENT DATA AT 60 ˚C

BTS Condition	Parameters	Oxygen loadings		
		63%	75%	80%
PBTS	τ (s)	9.9×10^7	1.3×10^7	1.1×10^6
	β	0.44	0.46	0.47
	E_τ(eV)	0.87	0.67	0.63
NBTS-recovery	τ (s)	7.9×10^8	1.9×10^9	2.6×10^6
	β	0.51	0.42	0.76
	E_τ(eV)	0.89	0.70	0.65

As the oxygen loadings increased, the peak energy barrier value was lowered down to 0.69 eV for the device with the oxygen loadings of 80%. Considering the spread of the Lorentz-shape distribution, the oxygen loadings-dependent behavior is consistent with those by stretched exponential analysis. The IGZO TFTs with 63% oxygen loadings had $E_{\tau,\text{PBTS}}$ and $E_{\tau,\text{NBTS recovery}}$ values of 0.87 and 0.89 eV, respectively. The oxygen vacancy might explain the positive V_{TH} shift of this device by the application of PBTS. The transition from the neutral V_O deep state to the double charge V_O^{2+} shallow state is a well-accepted mechanism for the negative V_{TH} shift under the negative bias illumination stress (NBIS) duration [10]–[12]. The reverse shallow-to-deep state transition of the V_O^{2+} defect can account for the qualitative positive V_{TH} shift under the PBTS duration because this transition consumes two free electrons. The transition model from V_O to V_O^{2+} basically involves the asymmetric energy barrier: in crystalline ZnO, the $E_{\tau,\text{NBTS}}$ value for the transition from the stable V_O to meta-stable V_O^{2+} is much greater than the $E_{\tau,\text{PBTS}}$ value from the metal-stable V_O^{2+} to stable V_O [18]. For example, the theoretically predicted $E_{\tau,\text{PBTS}}$ value for crystalline ZnO was rather low ($\sim$0.3 eV), which is similar to the experimentally determined $E_{\tau,\text{PBTS}}$ value ($\sim$0.3 eV) for amorphous Hf-In-Zn-O TFTs [28] on the basis of the shallow-to-deep transition of V_O^{2+}. Although the activation energy barrier for this transition of V_O^{2+} in a-IGZO system has not been explicitly calculated, Noh et $al.$ [8] showed that such a transition of V_O in a-IGZO can occur at even room temperature, implying that E_τ is not significantly large. In addition, most of V_O defect are deep donors in a-IGZO, which indicates they mostly exist in the neutral charge state initially [8]. Therefore, the shallow-to-deep transition of V_O for the device with 65% oxygen loadings is unlikely to be the origin of this V_{TH} shift under the PBTS condition. Very recently, the under-coordinated indium (In*) defect was suggested for electron trapping and bi-stable centers. According to this model, In*-metal (In*-M) exists in the neutral state in the pristine sample where it can trap excess electrons in the electron rich condition by the application of PBTS [normal state (NS) + 2e- $\leftrightarrow$ (In*-M)$^{2-}$] [30]. Similarly, In–Zn defect in oxygen deficient a-IGZO material was calculated to lie in the upper half of the bandgap as a gap state [31]. These M–M defects can be considered as V_O

This article has been accepted for inclusion in a future issue of this journal. Content is final as presented, with the exception of pagination.

ON *et al.*: ORIGIN OF ELECTRICAL INSTABILITIES

5

because they involve the missing oxygen. These identifications contradict the picture of V_O located in the lower half of the bandgap by Kamiya *et al.* [3]. The acceptor-like nature of the In*-M defect introduces the consumption of the free electron carriers, leading to the positive V_{TH} shift. It was noted that the energy barriers required in the configuration change depends on the E_F level. This defect would be responsible for high E_τ values (~0.9 eV) for the PBTS because its energy barrier for electron capture is 0.6–1.4 eV under the PBS condition. However, the emission barrier is 0.5–0.6 eV and therefore it is not satisfactory in explaining experimental results in full picture [30].

The comparable energy barriers of the PBTS- and NBTS recovery-induced V_{TH} instability strongly suggest the invocation of diffusion in the charged point defect. The ionic defects (e.g., Zn_i^{2+}, In_i^{3+}, and Ga_i^{3+}) or are likely to diffuse toward the back IGZO interface by the repulsive Columbic force during the PBTS duration, which can be greatly enhanced by the elevated temperature [25], [16]. This net displacement of the positively charged defects toward the back surface of IGZO films can cause either the simultaneous migration of associated electron carriers or the creation of negative image charges in the adjacent buffer layer on basis of charge density neutrality. The latter is not allowed because the insulating SiO_2 film in this paper was used as the buffer layer. Therefore, the reduction in effective free electron density near the gate dielectric/*a*-IGZO interface are responsible for the positive V_{TH} shift by PBTS [32]. In crystalline ZnO and In_2O_3, the effective migration energy barrier of Zn_i and In_i were ~0.5 eV [16] and 1.4–1.7 eV [33], respectively. Considering that the *a*-IGZO is an open structure compared to wurzite ZnO and bixbyite In_2O_3, the diffusional barriers of Zn_i and In_i are expected to be even lower (<0.5 eV and < 1.4 eV) [16], [33]. Thus, the migration of the Zn_i^{2+} or In_i^{3+} defects would affect the degradation of the device with 63% oxygen loadings.

In contrast, the *a*-IGZO TFTs with oxygen loadings of 75% and 80% had $E_{\tau,PBTS}$ values of 0.67 and 0.63 eV, respectively. The $E_{\tau,NBTS\ recovery}$ values for the recovery process was extracted to 0.70 and 0.65 eV for the devices with oxygen loadings of 75% and 80%, respectively. As discussed earlier, these rather low-energy barriers for the PBTS and NBTS recovery-induced V_{TH} instability cannot be reconciled by the oxygen vacancy [9], [10] or peroxide defects models [29]. The growing condition of high oxygen loadings would favor the formation of the oxygen interstitial [34] defect or the cation vacancy in the resulting IGZO film. According to the preliminary DFT calculation, the migration of oxygen interstitial [2]–[10], [13]–[19] is unlikely to be responsible for the rather low activation energy due to the required high diffusion barrier (>0.9 eV). In addition, one might expect that the trap/detrap of electrons from oxygen interstitial would give rise to the V_{TH} shifts under the PBTS and NBTS recovery conditions. Oxygen interstitials in *a*-IGZO have the following two distinct configurations depending on its charge state: the one loosely bound with neighboring metal ions in the 2- charge state (O_i^{2-}) and the dimer-like form (O_i^0) in the neutral state. In n-type *a*-IGZO material, O_i^{2-} is more stable

than O_i^0, indicating that they exist mainly in the 2- charge state in as-deposited films [18]. In principle, the O_i^0 in the neutral charge state can capture electrons, which would be responsible for PBTS-induced V_{TH} instability [35]. However, according to the formation energy diagram by Han *et al.* [36] oxygen interstitial prefers the 2- charge state with a viewpoint of thermodynamics under the n-type condition. This indicates that the dimer configuration with the neutral state is unlikely to be formed in as-deposited films. In contrast to O_i^0 which can capture excess electrons inducing bond-breaking relaxations, O_i^{2-} is not able to accept excess electrons implying that they cannot contribute to the device degradation under the initial PBTS condition. Therefore, the observed PBTS and NBTS recovery-induced V_{TH} instability is not accounted for by invoking oxygen interstitial. However, it does not necessarily mean that this mechanism can be completely excluded for plausible origin of the NBIS V_{TH} instability. Visible light or UV photon can activate the O_i^{2-} state into (O_i^0) with a donation of two delocalized electrons because of its high energy (>2 eV). It can be anticipated that the PBTS duration after NBIS duration (involving high-energy photon) would result in the different activation energy barriers.

Under the oxygen-rich condition, metal deficient sites (referred to as a metal vacancy V_M consistently with the terminology in the crystal phase) are expected to occur in the amorphous oxides. However, previous theoretical works reported that the formation energy of V_M in the isolated form is so high that it cannot be present for any sizable amount in the oxides [37], [38]. Instead, it could alternatively occur in a form of the complex defect with hydrogen ($NH - V_M$) where N is the number of hydrogens, which has a significant advantage over isolated hydrogen in terms of the formation energy [37], [38]. Note that the hydrogen concentration in the *a*-IGZO film is known to be $\geq 10^{20}$ cm^{-3}. Thus, these defects are expected to exist. We examined the energetics of ($NH - V_M$) in *a*-IGZO based on the DFT calculations using VASP code [43], [44]. In order to obtain physical insights into the electrical role of ($NH - V_M$), the defect formation energy (E^f) of ($NH - V_M$) with respect to its charge state were calculated as follows [37]:

$$E^f(d^q) = E_{tot}(d^q) - E_{tot}(clean) + \sum_i n_i \mu_i + q E_F \quad (3)$$

where $E_{tot}(d^q)$ and $E_{tot}(clean)$ are the total energies of a supercell including a defect with charge q (d^q) and without a defect, respectively. In (3), n_i is the number of the ith element which is added into or removed from the supercell and μ_i is its chemical potential which depends on the growth conditions. Since *a*-IGZO is meta-stable phase, chemical potentials ensuring its phase stability is not well defined. In this paper, the μ_i value was set to be zero and only focused on the relative formation energy of a defect between different charge states. E_F is referenced to the E_{VB}. Since the conventional PBE functional [45] underestimates the band gaps, we corrected band edge positions by considering the ratio of quasi-particle shifts of the band edges of *a*-IGZO [39] for the computed optical gap (2.03 eV) to match the experimental value (3.35 eV). We examined four configurations of ($NH - V_M$) for each
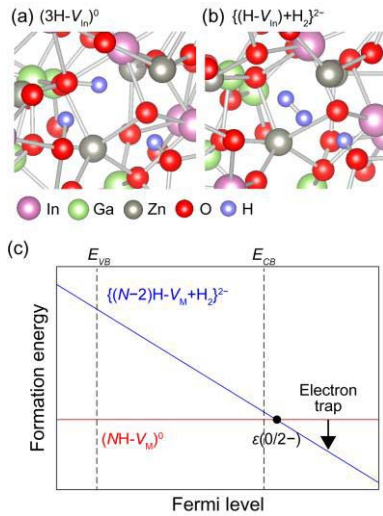
This article has been accepted for inclusion in a future issue of this journal. Content is final as presented, with the exception of pagination.

6   IEEE TRANSACTIONS ON ELECTRON DEVICES

Fig. 6. $(NH - V_M)^0$ different atomic configurations state. (a) Atomic structures of $(NH - V_M)^0$ for $M = $ In. (b) Electrons can lead to the binding between neighboring hydrogen ions, i.e., $2H^+ + 2e^- \rightarrow H_2$, which transforms $(NH - V_M)^0$ into $\{(N-2)H - V_M + H_2\}^{2-}$. (c) Change of the formation energies of $(NH - V_M)^0$ and $\{(N-2)H - V_M + H_2\}^{2-}$.

Fig. 7. Transition levels, $\varepsilon(0/2 -)$. Corresponding to the E_F level at which $\{(N-2)H - V_M + H_2\}^{2-}$ begins to be more stable than $(NH - V_M)^0$.

Fig. 8. Calculated configuration coordination diagram describing the transformation from $(3H - V_{In})^0$ into $\{(H - V_{In}) + H_2\}^{2-}$. (a) $E_F = E_{CB} + 0.74$ eV and (b) $E_F = E_{CB} + 0.21$ eV. E_{trap} and E_{detrap} are the energy barriers for electron trap and detrap process, respectively. E_{rot} is the activation energy for the rotation of H_2 molecule.

metal type. According to recent DFT calculations [38], $(2H - V_{Zn})$, which fully passives holes in V_{Zn}, has the lowest energy compared to configurations with other N under typical growth conditions. Hence, we selected N as 3 for In and Ga and 2 for Zn.

In the neutral charge state of $(NH - V_M)^0$, a hydrogen atom forms an O-H bond with the oxygen atom in V_M. Fig. 6(a) shows one of the atomic structures of $(NH - V_M)^0$ for $M = $ In. Meanwhile, the presence of excess electrons can lead to binding between neighboring hydrogen ions, i.e., $2H^+ + 2e^- \rightarrow H_2$, which transforms $(NH - V_M)^0$ into $\{(N-2)H - V_M + H_2\}^{2-}$, as shown in Fig. 6(b). The stable charge state of defects depends on the E_F level. The variations in the formation energies of $(NH - V_M)^0$ and $\{(N-2)H - V_M + H_2\}^{2-}$ as a function of the E_F level were schematically shown in Fig. 6(c). The formation energy of $(NH - V_M)^0$ is smaller than that of $\{(N-2)H - V_M + H_2\}^{2-}$ for the E_F less than the E_{CB}. However, the formation energy of $\{(N-2)H - V_M + H_2\}^{2-}$ is reduced with increasing E_F level. Thus, the reversal of the stability between two charge states can occur when the E_F lies near E_{CB}. Fig. 7 shows the calculated transition levels $[\varepsilon (0/2-)]$ for these defects where $\{(N-2)H - V_M + H_2\}^{2-}$ begins to be more stable than $(NH - V_M)^0$. The $\varepsilon (0/2-)$ can be found to be higher than $E_{CB} - 0.2$ eV. It means that most of $(NH - V_M)$ in the a-IGZO film initially exists in the neutral charge state because the E_F typically lies 0.1–0.2 eV below the E_{CB} in the pristine IGZO film. The application of PBTS allows the E_F in a channel close to the gate dielectric effectively to move upward above E_{CB} due to the band bending. Positioning of E_F above the $\varepsilon (0/2-)$s of $(NH-V_M)$ causes the $\{(N-2)H - V_M + H_2\}^{2-}$ state to be energetically favored than $(NH - V_M)^0$, which drives the transformation of the defect configuration from $(NH - V_M)^0$ into $\{(N-2)H - V_M + H_2\}^{2-}$. Once $\{(N-2)H - V_M + H_2\}^{2-}$ occurs in a-IGZO film, V_{TH} shifts to the positive direction
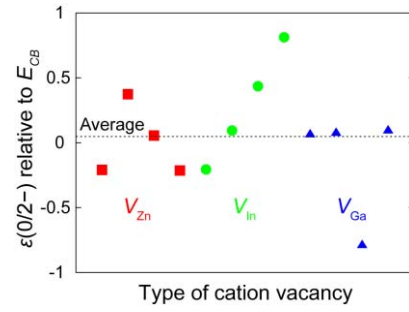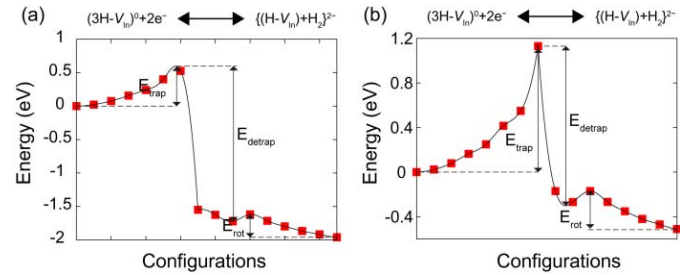
because its negative charge screens the electric field to attract electrons to the interface.

Next, the activation energy of electron trap/detrap process by $(NH - V_M)$ defects was examined. To this end, we considered In vacancy which is known to be more stable in energetics than Ga and Zn vacancy in crystalline InGaZnO$_4$ [40]. Fig. 8(a) shows the calculated configuration coordination diagram describing the transformation from $(3H - V_{In})^0$ into $\{H - V_{In} + H_2\}^{2-}$ under the PBTS condition. E_τ values were calculated by nudged elastic bandmethod, considering extra electrons in the CB. It leads to the E_F level to be at $E_{CB} + 0.74$ eV (Fig. 8). This E_F level corresponds to a free electron density of 5×10^{20} cm^{-3}, which is consistent with that of a-IGZO film in the on state. The thermal energy barrier for the formation of $\{H - V_{In} + H_2\}^{2-}$ is calculated as $\sim$0.53 eV, which is in reasonable agreement with 0.63–0.67 eV for the positive shift of V_{TH} of the films deposited under an oxygen-rich condition in the experiments. Note that the configuration coordination diagram varies depending on the E_F; the E_F in calculation must lie below E_{CB} for reproducing carrier concentration in the devices under NBTS. Thus, the E_τ ($\sim$2.49 eV) for the reverse reaction shown in Fig. 8 do not exactly correspond to the experimental energy barrier of the negative shift of V_{TH} under the NBTS condition. Under the NBTS condition, $(3H - V_{In})^0$ is energetically preferred to $\{(H - V_{In}) + H_2\}^{2-}$ due to the downward E_F, and the thermal energy barrier for $\{(H - V_{In}) + H_2\}^{2-} \rightarrow (3H - V_{In})^0 + 2e^-$ will be smaller than that under the PBTS condition [41]. Indeed, it was found that the energy barriers for the electron
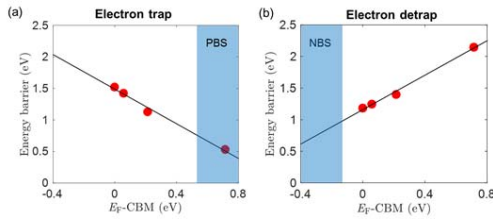
ON *et al.*: ORIGIN OF ELECTRICAL INSTABILITIES

7

This article has been accepted for inclusion in a future issue of this journal. Content is final as presented, with the exception of pagination.

Fig. 9. Change of energy barriers as a function of the Fermi level for electron (a) trap and (b) detrap process.

emission by $\{(H - V_{In}) + H_2\}^{2-}$ are 0.5–0.9 eV for the E_F lying 0.4–0.1 eV below the E_{CB}, which is a range of E_F under the NBTS condition [Fig. 9]. Owing to this low barrier, molecular hydrogen can emit electrons into E_F leading to the dissociation of hydrogen bond even at low temperatures (25 °C–100 °C) used in experiments. The $(NH - V_M)$ model in this paper can also be applicable in bottom gate a-IGZO TFTs because this defect is one of the intrinsic defects in hydrogen-rich a-IGZO material.

After the dissociation of hydrogen molecule, H atom can return to the different sites around the same cation vacancy, which can affect energy barriers slightly. In addition, one may still concern the diffusion of the dissociated hydrogen to other sites escaping the original vacancy site. However, the energy required for the removal of a hydrogen leading to $(NH - V_M)^0 \rightarrow \{(N - 1)H - V_M\}^{1-} + H_i^+$ is found to be 0.26 eV. Therefore, we expect that the attractive interaction between $\{(N-1)H - V_M\}^{1-}$ and H_i^+ does not make an H atom in the defect complex to be highly mobile. In the reference [19], an impact of hydrogen interstitial (H_i) as well as hydrogen substitution on oxygen site (H_O) on the device instability were discussed based on the O-deficient IZTO. In this paper, the role of hydrogen impurity was investigated for O-excess IGZO samples. In particular, microscopic mechanism which can explain the relatively low-energy barrier for the electron capture in O-excess samples have been suggested.

It is noted that the rationale of PBTS and NBTS instabilities of the a-IGZO TFTs was mainly discussed on basis of the intrinsic defects in the a-IGZO film. It does not necessarily mean the exclusion of the extrinsic degradation mechanisms such as the charge injection into the bulk gate dielectric and charge trapping near the SiO_2/a-IGZO interface. Recently, the point defects for the a-IGZO/SiO_2 interface were calculated to be similar to the bulk defects in a-IGZO where the M-O bond lengths (M = In or Ga) at the interface of SiO_2/a-IGZO and bulk a-IGZO film have no significant difference, suggesting that the intrinsic defects model including cation vacancy defects would be extended even at the a-IGZO/SiO_2 interface [42]. In contrast, the charge injection model may be ruled out because the energy barrier required for the accumulated electrons to be injected into the gate dielectric with high bandgap (~8 eV) under PBTS is obviously different from that for the recovery process such as emission of captured electrons, which cannot explain the similar energy barriers for the PBTS and recovery process for the IGZO TFTs. Finally, it is also noted that the (NH-V_M) model in this paper can also

be applicable in bottom gate IGZO TFTs because this defect is one of the intrinsic defects in hydrogen-rich IGZO material.

IV. CONCLUSION

In summary, the electrical properties of a-IGZO TFTs with a self-aligned coplanar structure were investigated, where the oxygen loadings in the a-IGZO channel layer was varied to 63%, 75%, and 80%. The slightly decreasing μ_{FE} and positively displaced V_{TH} variations for the a-IGZO TFTs with increasing oxygen loadings were attributed to the reduction in V_O density and the increase in CB offset. The positive V_{TH} shift by the application of PBTS for the a-IGZO TFTs was amplified with increasing oxygen loadings. The energy barriers ($E_{\tau,PBTS}$) responsible for the degradation of the devices with oxygen loadings of 63%, 75%, and 80% were 0.87, 0.67, and 0.63 eV, respectively. The activation energy barriers for the recovery process (by NBTS) exhibited a similar trend. The $E_{\tau,NBTS\ Recovery}$ values for the devices with oxygen loadings of 63%, 75%, and 80% were 0.89, 0.70, and 0.65 eV, respectively. The origin of the former can be attributed to the migration of the cation interstitial defect. Conversely, the new degradation mechanism of the $(NH - V_M)$ defect center was identified for the devices with the higher oxygen loadings (75% and 80%) based on the DFT calculation. This finding provides a comprehensive framework to understand the gate bias thermal stress induced instabilities of the technically important a-IGZO TFTs.

REFERENCES

[1] E. Fortunato, P. Barquinha, and R. Martins, "Oxide semiconductor thin-film transistors: A review of recent advances," *Adv. Mater.*, vol. 24, no. 22, pp. 2945–2986, Jun. 2012.
[2] J. C. Park *et al.*, "Highly stable transparent amorphous oxide semiconductor thin-film transistors having double-stacked active layers," *Adv. Mater.*, vol. 22, no. 48, pp. 5512–5516, Dec. 2010.
[3] T. Kamiya, K. Nomura, and H. Hosono, "Present status of amorphous In–Ga–Zn–O thin-film transistors," *Sci. Technol. Adv. Mater.*, vol. 11, no. 4, p. 044305, Sep. 2011.
[4] K. Nomura, H. Ohta, A. Takagi, T. Kamiya, M. Hirano, and H. Hosono, "Room-temperature fabrication of transparent flexible thin-film transistors using amorphous oxide semiconductors," *Nature*, vol. 432, no. 4016, pp. 488–492, Nov. 2004.
[5] S. Oh, J. H. Baeck, J. U. Bae, K.-S. Park, and I. B. Kang, "Effect of interfacial excess oxygen on positive-bias temperature stress instability of self-aligned coplanar InGaZnO thin-film transistors," *Appl. Phys. Lett.*, vol. 108, no. 14, p. 141604, Apr. 2016.
[6] J. K. Jeong, "The status and perspectives of metal oxide thin-film transistors for active matrix flexible displays," *Semicond. Sci. Technol.*, vol. 26, no. 3, p. 034008, Feb. 2011.
[7] A. Janotti and C. G. Van de Walle, "Oxygen vacancies in ZnO," *Appl. Phys. Lett.*, vol. 87, no. 12, p. 122102, Sep. 2005.
[8] H.-K. Noh, K. J. Chang, B. Ryu, and W.-J. Lee, "Electronic structure of oxygen-vacancy defects in amorphous In-Ga-Zn-O semiconductors," *Phys. Rev. B, Condens. Matter*, vol. 84, no. 11, p. 115205, Sep. 2011.
[9] J. K. Jeong, "Photo-bias instability of metal oxide thin film transistors for advanced active matrix display," *J. Mater. Res.*, vol. 28, no. 16, pp. 2071–2084, Aug. 2013.
[10] M. D. H. Chowdhury, P. Migliorato, and J. Jang, "Light induced instabilities in amorphous indium–gallium–zinc–oxide thin-film transistors," *Appl. Phys. Lett.*, vol. 97, no. 17, p. 173506, Oct. 2010.
[11] S. Yang *et al.*, "Suppression in the negative bias illumination instability of Zn-Sn-O transistor using oxygen plasma treatment," *Appl. Phys. Lett.*, vol. 99, no. 10, p. 102103, Aug. 2011.
[12] M. D. H. Chowdhury, P. Migliorato, and J. Jang, "Temperature dependence of negative bias under illumination stress and recovery in amorphous indium gallium zinc oxide thin film transistors," *App. Phys. Lett.*, vol. 102, no. 14, p. 143506, Apr. 2013.

This article has been accepted for inclusion in a future issue of this journal. Content is final as presented, with the exception of pagination.

8   IEEE TRANSACTIONS ON ELECTRON DEVICES

[13] H. Oh, S.-M. Yoon, M. K. Ryu, C.-S. Hwang, S. Yang, and S.-H. K. Park, "Photon-accelerated negative bias instability involving subgap states creation in amorphous In–Ga–Zn–O thin film transistor," *Appl. Phys. Lett.*, vol. 97, no. 18, p. 183502, Nov. 2010.

[14] B. S. Yang *et al.*, "Improvement of the photo-bias stability of the Zn–Sn–O field effect transistors by an ozone treatment," *J. Mater. Chem.*, vol. 22, no. 22, pp. 10994–10998, Apr. 2010.

[15] K. H. Ji *et al.*, "Effect of high-pressure oxygen annealing on negative bias illumination stress-induced instability of InGaZnO thin film transistors," *Appl. Phys. Lett.*, vol. 98, no. 10, p. 103509, Mar. 2011.

[16] Y.-M. Kim *et al.*, "Investigation of zinc interstitial ions as the origin of anomalous stress-induced hump in amorphous indium gallium zinc oxide thin film transistors," *Appl. Phys. Lett.*, vol. 102, no. 17, p. 173502, Apr. 2013.

[17] K. Ide, Y. Kikuchi, K. Nomura, M. Kimura, T. Kamiya, and H. Hideo, "Effects of excess oxygen on operation characteristics of amorphous In-Ga-Zn-O thin-film transistors," *Appl. Phys. Lett.*, vol. 99, no. 9, p. 093507, Sep. 2011.

[18] J. Robertson and Y. Guo, "Light induced instability mechanism in amorphous InGaZn oxide semiconductors," *Appl. Phys. Lett.*, vol. 104, no. 15, p. 162102, Apr. 2014.

[19] Y. Kang *et al.*, "Hydrogen bistability as the origin of photo-bias-thermal instabilities in amorphous oxide semiconductors," *Adv. Electron. Mater.*, vol. 1, no. 7, p. 1400006, Jul. 2015.

[20] P. S. Andry and F. R. Libsch, "Method for fabricating self-aligned thin-film transistors to define a drain and source in a single photolithographic step," U.S. Patent 6 338 988, Jan. 15, 2002.

[21] C. Chen, K. Abe, H. Kumomi, and J. Kanicki, "Density of states of a-InGaZnO from temperature-dependent field-effect studies," *IEEE Trans. Electron Devices*, vol. 56, no. 6, pp. 1177–1183, Jun. 2009.

[22] R. Schumacher, P. Thomas, K. Weber, and W. Fuhs, "The Meyer–Neldel rule in field-effect measurements and the microscopic prefactor of the conductivity in a-Si:H," *Solid State Commun.*, vol. 62, no. 1, pp. 15–17, Apr. 1987.

[23] H. Overhof, "The prefactor of the dc conductivity in amorphous semiconductors," *J. Non-Cryst. Solids*, vols. 97–98, pp. 539–542, Dec. 1987.

[24] K. H. Ji *et al.*, "The effect of density-of-state on the temperature and gate bias-induced instability of InGaZnO thin film transistors," *J. Electrochem. Soc.*, vol. 157, no. 11, pp. H983–H986, Sep. 2010.

[25] M. D. H. Chowdhury, P. Migliorato, and J. Jang, "Time-temperature dependence of positive gate bias stress and recovery in amorphous indium-gallium-zinc-oxide thin-film-transistors," *Appl. Phys. Lett.*, vol. 98, no. 15, p. 153511, Apr. 2011.

[26] S. G. J. Mathijssen *et al.*, "Dynamics of threshold voltage shifts in organic and amorphous silicon field-effect transistors," *Adv. Mater.*, vol. 19, no. 19, pp. 2785–2789, Aug. 2007.

[27] S. Lee, A. Nathan, S. Jeon, and J. Robertson, "Oxygen defect-induced metastability in oxide semiconductors probed by gate pulse spectroscopy," *Sci. Rep.*, vol. 5, Oct. 2015, Art. no. 14902.

[28] K. Ghaffarzadeh *et al.*, "Persistent photoconductivity in Hf–In–Zn–O thin film transistors," *Appl. Phys. Lett.*, vol. 97, no. 14, p. 143510, Oct. 2010.

[29] H.-H. Nahm, Y.-S. Kim, and D. H. Kim, "Instability of amorphous oxide semiconductors via carrier-mediated structural transition between disorder and peroxide state," *Phys. Status Solidi B*, vol. 249, no. 6, pp. 1277–1281, Jun. 2012.

[30] H.-H. Nahm and Y.-S. Kim, "Undercoordinated indium as an intrinsic electron-trap center in amorphous InGaZnO4," *NPG Asia Mater.*, vol. 6, p. e143, Nov. 2014.

[31] W. Körner, D. F. Urban, and C. Elsässer, "Origin of subgap states in amorphous In-Ga-Zn-O," *J. Appl. Phys.*, vol. 114, no. 16, p. 163704, Oct. 2013.

[32] H. Oh, S.-H. K. Park, C.-S. Hwang, S. Yang, and M. K. Ryu, "Enhanced bias illumination stability of oxide thin film transistor through insertion of ultrathin positive charge barrier into active material," *Appl. Phys. Lett.*, vol. 99, no. 2, p. 022105, Jul. 2011.

[33] P. Ágoston and K. Albe, "*Ab initio* modeling of diffusion in indium oxide," *Phys. Rev. B, Condens. Matter*, vol. 81, p. 195205, May 2010.

[34] A. Janotti and C. G. Van de Walle, "Oxygen vacancies in ZnO," *Appl. Phys. Lett.*, vol. 87, no. 12, p. 122102, Sep. 2005.

[35] S. Oh, J. H. Baeck, H. S. Shin, J. U. Bae, K.-S. Park, and I. B. Kang, "Comparison of top-gate and bottom-gate amorphous InGaZnO thin-film transistors with the same SiO2/a-InGaZnO/SiO2 stack," *IEEE Electron Device Lett.*, vol. 35, no. 10, pp. 1037–1039, Oct. 2014.

[36] W. H. Han, Y. J. Oh, K. J. Chang, and J.-S. Park, "Electronic structure of oxygen interstitial defects in amorphous In-Ga-Zn-O semiconductors and implications for device behavior," *Phys. Rev. Appl.*, vol. 3, p. 044008, Apr. 2015.

[37] J. B. Varley, H. Peelaers, A. Janotti, and C. G. Van de Walle, "Hydrogenated cation vacancies in semiconducting oxides," *J. Phys., Condens. Matter*, vol. 23, no. 33, p. 334212, Aug. 2011.

[38] Y. Kang, H.-H. Nahm, and S. Han, "Light-induced peroxide formation in ZnO: Origin of persistent photoconductivity," *Sci. Rep.*, vol. 6, Oct. 2016, Art. no. 35148.

[39] Y. Kang, H. Song, H.-H. Nahm, S. H. Jeon, Y. Cho, and S. Han, "Intrinsic nature of visible-light absorption in amorphous semiconducting oxides," *APL Mater.*, vol. 2, no. 3, p. 032108, Mar. 2014.

[40] A. Murat, A. U. Adler, T. O. Mason, and J. E. Medvedeva, "Carrier generation in multicomponent wide-bandgap oxides: InGaZnO4," *J. Amer. Chem. Soc.*, vol. 135, no. 15, pp. 5685–5692, Mar. 2013.

[41] K. Nomura, T. Kamiya, and H. Hosono, "Effects of diffusion of hydrogen and oxygen on electrical properties of amorphous oxide semiconductor, In-Ga-Zn-O," *ECS J. Solid State Sci. Technol.*, vol. 2, no. 1, pp. P5–P8, Nov. 2013.

[42] H. Song, Y. Kang, H. H. Nahm, and S. Han, "Source of instability at the amorphous interface between InGaZnO4 and SiO2: A theoretical investigation," *Phys. Status Solidi B*, vol. 252, no. 8, pp. 1872–1876, Aug. 2015.

[43] G. Kresse and J. Furthmüller, "Efficient iterative schemes for *ab initio* total-energy calculations using a plane-wave basis set," *Phys. Rev. B, Condens. Matter*, vol. 54, no. 16, pp. 11169–11189, Oct. 1996.

[44] G. Kresse and D. Joubert, "From ultrasoft pseudopotentials to the projector augmented-wave method," *Phys. Rev. B, Condens. Matter*, vol. 59, no. 3, pp. 1758–1775, Jan. 1996.

[45] J. P. Perdew, K. Burke, and M. Ernzerhof, "Generalized gradient approximation made simple," *Phys. Rev. Lett.*, vol. 77, no. 18, pp. 3865–3868, Oct. 1996.

Nuri On is currently pursuing the Ph.D. degree with the Department of Electronic Engineering, Hanyang University, Seoul, South Korea.

Youngho Kang received the Ph.D. degree in in material science and engineering from Seoul National University, Seoul, South Korea, in 2015.
He is a Post-Doctoral Researcher with Material Department, University of California, Santa Barbara, CA, USA.

Aeran Song is currently pursuing the Ph.D. degree from the Division of Physics and Semiconductor Science, Dongguk University, Seoul, South Korea.

Byung Du Ahn received the Ph.D. degree in the Department of Electronic Engineering from Yonsei University, Seoul, South Korea.
He is a Senior Researcher of the oxide TFT-based AMOLED TV group with Samsung Display, Asan, South Korea.

Hye Dong Kim received the Ph.D. degree in the Department of Materials Science and Engineering from Korea Advanced Institute of Science and Technology, Daejeon, South Korea.
He is in charge of the oxide TFT-based AMOLED TV with Samsung Display Inc., Asan, South Korea.

Jun Hyung Lim received the Ph.D. degree in the Department of Materials Science and Engineering from Sungkyunkwan University, Suwon, South Korea, in 2006.
He is in charge of the oxide backplane with the Research and Development Center, Samsung Display, Yongin, South Korea.

Kwun-Bum Chung received the Ph.D. degree in the Institute of Physics and Applied Physics from Yeosei University, Seoul, South Korea, in 2006.

He is an Associated Professor with the Division of Physics and Semiconductor Science, Dongguk University, Seoul, South Korea.

Seungwu Han received the Ph.D. degree in the Department of Physics, Seoul National Univerity, Seoul, South Korea, in 2000.

He is a Professor with the Department of Materials Science and Engineering, Seoul National University, Seoul, South Korea.

Jae Kyeong Jeong received the Ph.D. degree in the Department of Materials Science and Engineering from Seoul National University, Seoul, South Korea, in 2002.

He is a Professor with the Department of Electronic Engineering, Hanyang University, Seoul, South Korea.